

# Mass measurements of $^{22}\text{Mg}$ and $^{26}\text{Si}$ via the $^{24}\text{Mg}(p,t)^{22}\text{Mg}$ and $^{28}\text{Si}(p,t)^{26}\text{Si}$ reactions

A. Parikh,<sup>1</sup> J. A. Caggiano,<sup>1,\*</sup> C. Deibel,<sup>1</sup> J. P. Greene,<sup>2</sup> R. Lewis,<sup>1</sup> P. D. Parker,<sup>1</sup> and C. Wrede<sup>1</sup>

<sup>1</sup>Wright Nuclear Structure Laboratory, Yale University, New Haven, Connecticut 06520, USA

<sup>2</sup>Physics Division, Argonne National Laboratory, Argonne, Illinois 60439, USA

(Received 31 January 2005; published 19 May 2005)

Using a 33 MeV proton beam with our Enge split-pole spectrograph, we measured the  $Q_0$  values of the  $^{24}\text{Mg}(p,t)^{22}\text{Mg}$  and  $^{28}\text{Si}(p,t)^{26}\text{Si}$  reactions relative to that of the  $^{16}\text{O}(p,t)^{14}\text{O}$  reaction. Data were obtained at scattering angles of  $15^\circ$  and  $25^\circ$ . Based on the masses of  $^{24}\text{Mg}$ ,  $^{28}\text{Si}$ ,  $^{16}\text{O}$ ,  $^{14}\text{O}$ ,  $p$ , and  $t$ , we determined the mass excesses of  $^{22}\text{Mg}$  and  $^{26}\text{Si}$  to be  $-400.5(1.0)$  and  $-7139.5(1.0)$  keV, respectively. Our result for the mass of  $^{22}\text{Mg}$  is in excellent agreement with recent high-precision measurements.

DOI: 10.1103/PhysRevC.71.055804

PACS number(s): 21.10.Dr, 26.30.+k, 27.30.+t, 25.40.Hs

## I. INTRODUCTION

The detection of characteristic  $\gamma$ -ray lines of astrophysical origin allows important nuclear physics constraints to be set on nucleosynthesis models of astrophysical phenomena. The 1.809 and 1.275 MeV  $\beta$ -delayed  $\gamma$  rays from  $^{26}\text{Al}_{(\text{g.s.})}$  ( $t_{1/2} = 7.2 \times 10^5$  yr) and  $^{22}\text{Na}$  ( $t_{1/2} = 2.6$  yr), respectively, constitute two of these production signatures for which searches have been conducted (see, e.g. [1] for others). While the former has been widely observed in our Galaxy by several satellites, including NASA's CGRO and ESA's INTEGRAL [2,3], the latter has not yet been seen [4,5]. Reproducing these observations (or lack thereof) through simulations of explosions (novae, supernovae) or stars suffering gross mass loss [such as asymptotic giant branch (AGB) or Wolf-Rayet stars] requires knowledge of the relevant temperatures and densities involved, as well as those reaction rates that can influence the production and destruction of these nuclei in these environments. In particular, for evaluating the contribution of novae to the abundances of  $^{22}\text{Na}$  and  $^{26}\text{Al}_{(\text{g.s.})}$ , much recent experimental work has been concentrated on determining the rates of the reactions  $^{21}\text{Na}(p,\gamma)^{22}\text{Mg}$  (see, e.g. [6] for a summary) and  $^{25}\text{Al}(p,\gamma)^{26}\text{Si}$  [7–9], respectively, at the prompting of the astrophysics community [10,11].

The resonant component of a nuclear reaction rate depends exponentially on the resonance energy  $E_R = E_x - Q_0$ , where  $E_x$  is the excitation energy of a state in the compound nucleus and  $Q_0$  is the ground-state  $Q$  value of the reaction. Direct reaction rate determinations involve explicit experimental measurements of  $E_R$ ; indirect determinations use experiments to determine  $E_x$  and use the masses of the nuclei involved to find  $Q_0$ .

The recent direct measurement of the  $^{21}\text{Na}(p,\gamma)^{22}\text{Mg}$  reaction at TRIUMF-ISAC [12] pointed to a disagreement between their measured value of  $E_R = 205.7(5)$  keV and the literature value of  $E_x - Q_0 = 212(2)$  keV [13,14] for the  $E_x = 5.71$  MeV state in  $^{22}\text{Mg}$ . This prompted a reexamination of an earlier determination of the  $^{22}\text{Mg}$  mass [15,16], two high-precision studies of the mass of this nucleus using

Penning traps [17,18], and two new  $\gamma$ -ray measurements of the excitation energy of this state [19,20]. These results are summarized in Tables I and II and Fig. 1. Thanks to these efforts, a consistent set of results that resolves the discrepancy is now emerging. However, this example forces us to reexamine other indirect determinations of reaction rates where one or more of the nuclei involved have uncertain masses ( $\geq 1$  keV). Precise mass values are needed because of the exponential dependence of the reaction rate on  $Q_0$ .

The nucleus  $^{26}\text{Si}$  is listed in the most recent mass evaluation [14] with a mass excess  $\Delta = M - A = -7145(3)$  keV. As mentioned above, the rate of the  $^{25}\text{Al}(p,\gamma)^{26}\text{Si}$  reaction represents one of the key uncertainties in determining whether novae are viable astrophysical sites for the production of the  $\beta$ -delayed  $\gamma$ -emitter  $^{26}\text{Al}_{(\text{g.s.})}$  [11]. Recent indirect studies of the structure of  $^{26}\text{Si}$  above the  $^{25}\text{Al} + p$  threshold (and corresponding indirect determinations of the rate) have been made [7–9], and a direct study of the  $^{25}\text{Al}(p,\gamma)^{26}\text{Si}$  reaction at TRIUMF-ISAC has been proposed [21]. Therefore, it is important to revisit the question of the mass of  $^{26}\text{Si}$ .

## II. EXPERIMENT AND RESULTS

We determined the masses of  $^{26}\text{Si}$  and  $^{22}\text{Mg}$  by studying the  $^{28}\text{Si}(p,t)^{26}\text{Si}$ ,  $^{24}\text{Mg}(p,t)^{22}\text{Mg}$ , and  $^{16}\text{O}(p,t)^{14}\text{O}$  reactions and detecting the tritons corresponding to the ground states of  $^{26}\text{Si}$ ,  $^{22}\text{Mg}$ , and  $^{14}\text{O}$ . Using the measured energies of these tritons, along with the beam energy and scattering angle, we determined the  $Q_0$  values of the  $^{28}\text{Si}(p,t)^{26}\text{Si}$  and  $^{24}\text{Mg}(p,t)^{22}\text{Mg}$  reactions relative to that of the  $^{16}\text{O}(p,t)^{14}\text{O}$  reaction. Assuming the most recent mass evaluation values for the other relevant nuclei [14], we then found the masses of  $^{26}\text{Si}$  and  $^{22}\text{Mg}$ .

The tandem Van de Graaff accelerator at Yale University's Wright Nuclear Structure Laboratory produced a 33 MeV beam of protons that was delivered to the target position of our Enge split-pole spectrometer. Measurements were made at nominal scattering angles of  $15^\circ$  and  $25^\circ$ ; the acceptance was  $\Delta\Theta = \pm 10$  mrad,  $\Delta\Phi = \pm 40$  mrad; and the magnetic field was chosen to place the tritons corresponding to both the  $^{26}\text{Si}$  and  $^{22}\text{Mg}$  ground states in roughly the center of our focal

\*Present address: TRIUMF, Vancouver, British Columbia, Canada V6T 2A3.

TABLE I. Recent direct and derived determinations of the mass excess ( $M - A$ ) of  $^{22}\text{Mg}$ . Note that in deriving the mass excess of  $^{22}\text{Mg}$  from  $E_R$  and  $E_x$  we assumed the mass excesses of  $^{21}\text{Na}$  and  $p$  from [14].

Study	$^{22}\text{Mg}$ mass excess (keV)
2003 mass evaluation [14]	-397.0 (1.3)
Recent reevaluation of older data [15,16]	-402 (3)
CPT [17]	-399.73 (67)
ISOLTRAP [18]	-399.92 (27)
TRIUMF $E_R + E_x$ of 5.71 MeV state from literature [12,13]	-403.4 (1.5)
TRIUMF $E_R +$ recent $\gamma$ -ray measurement of 5.71 MeV state [12,19]	-400.5 (1.3)
TRIUMF $E_R +$ recent $\gamma$ -ray measurement of 5.71 MeV state [12,20]	-398.8 (3.3)
Present work	-400.5 (1.0)

plane detector. We employed a  $65 \mu\text{g}/\text{cm}^2$   $^{28}\text{SiO}$  target with a gold flash and a  $67 \mu\text{g}/\text{cm}^2$   $^{24}\text{MgO}$  target on a  $15 \mu\text{g}/\text{cm}^2$  natural carbon backing for our  $(p,t)$  measurements. In addition, we used a  $360 \mu\text{g}/\text{cm}^2$   $^{25}\text{MgO}$  target and a  $140 \mu\text{g}/\text{cm}^2$  Al target for momentum calibration of the focal plane through the  $^{25}\text{Mg}(p,d)^{24}\text{Mg}$  and  $^{27}\text{Al}(p,d)^{26}\text{Al}$  reactions. Both  $(p,t)$  measurements [along with the  $(p,d)$  measurements] were made in the same experimental run, with unchanged beam energy, scattering angle (for each of the two angles employed), and magnetic field. Hence, the same momentum calibration can be used to determine the  $Q_0$  value of both the  $^{28}\text{Si}(p,t)^{26}\text{Si}$  and  $^{24}\text{Mg}(p,t)^{22}\text{Mg}$  reactions.

TABLE II.  $\gamma$ -ray energy measurements from the  $E_x = 5.71$  MeV state in  $^{22}\text{Mg}$ .

Source	$\gamma$ -ray energy from $E_x = 5.71$ MeV state in $^{22}\text{Mg}$ (keV)
1990 compilation [13]	5713.9(1.2)
New ANL measurement [19]	5711.0(1.0)
New ORNL measurement [20]	5709.3(3.2)

The focal plane detection system consisted of a position-sensitive gas ionization drift chamber, followed by a scintillator; it will be described in detail elsewhere [22], but it is similar in design and operation to that described in [23]. The focal plane detector provides two position measurements (via lumped delay-line readouts) and a cathode ( $\Delta E$ ) signal, while the scintillator provides a residual energy measurement. With these signals, we were able to identify and separate the various particle groups (protons, deuterons, tritons, and alphas) in our reactions.

Figure 2(a) shows the triton momentum spectrum from the  $^{28}\text{Si}(p,t)^{26}\text{Si}$  reaction at  $15^\circ$ . Tritons corresponding to the ground and first excited states of  $^{26}\text{Si}$  are clearly seen, along with contaminant peaks from the  $^{12}\text{C}(p,t)^{10}\text{C}$  and  $^{16}\text{O}(p,t)^{14}\text{O}$  reactions (leading to the ground states of  $^{10}\text{C}$  and  $^{14}\text{O}$ , respectively). Figure 2(b) shows the triton momentum spectrum from the  $^{24}\text{Mg}(p,t)^{22}\text{Mg}$  reaction at  $15^\circ$ ; again, we see the contaminant  $^{12}\text{C}(p,t)$  and  $^{16}\text{O}(p,t)$  peaks flanking the peak corresponding to the ground state of  $^{22}\text{Mg}$ . The energy resolution, determined using the  $^{22}\text{Mg}$  ground-state peak, is 10 keV full width at half maximum. The spectra in Figs. 2(a) and 2(b) represent about 20 and 13 h of data, respectively, at a proton beam intensity of about 20 nA. The

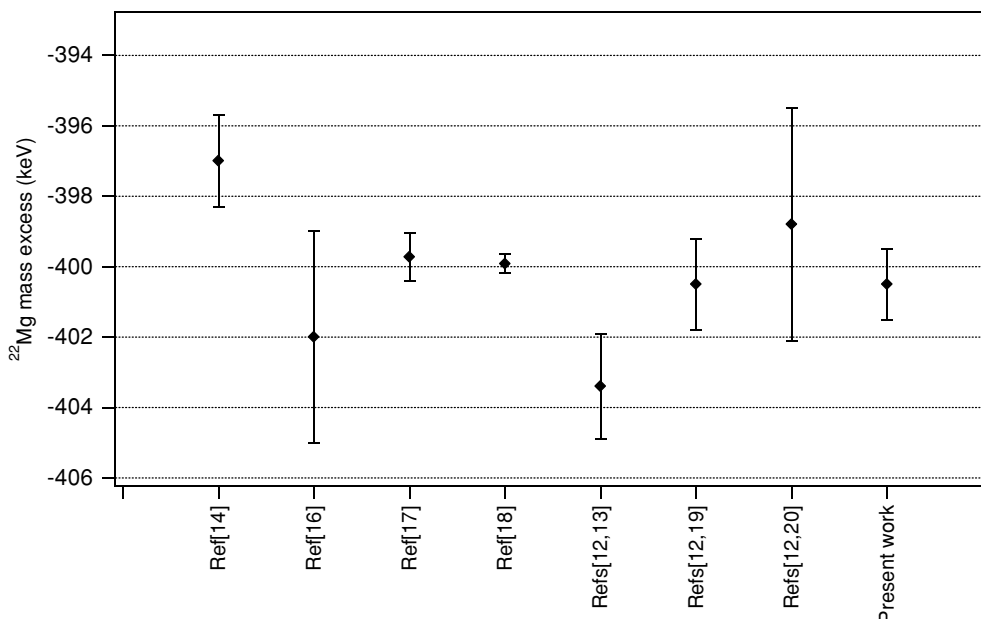


FIG. 1. Recent direct and derived determinations of the  $^{22}\text{Mg}$  mass excess. See also Table I and Sec. III of the text.

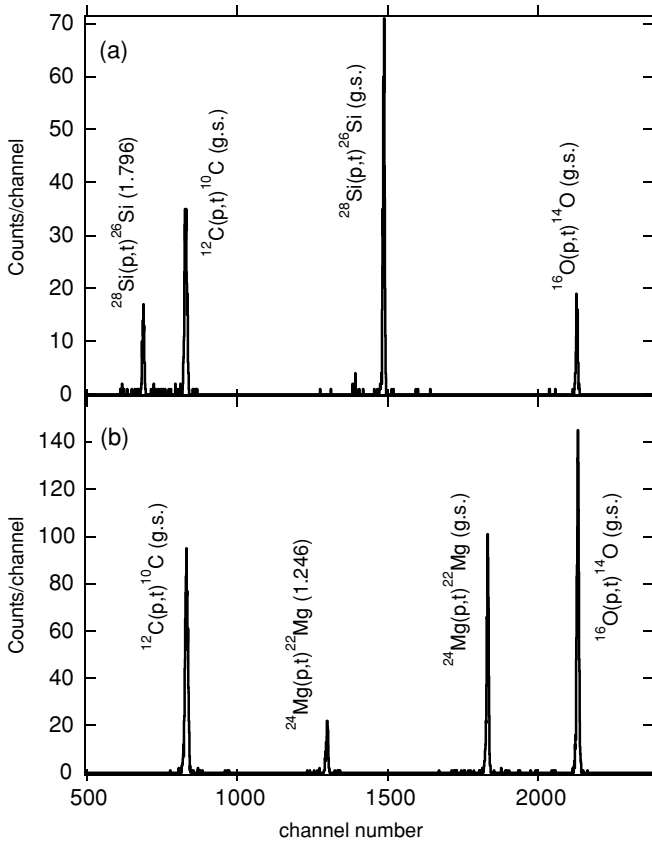


FIG. 2. Triton momentum spectra (at  $\theta = 15^\circ$ ) from  $(p,t)$  reactions on (a) the  $^{28}\text{SiO}$  target and (b) the  $^{24}\text{MgO} + \text{C}$  target.

triton spectra at  $25^\circ$  were similar to those at  $15^\circ$ . Both Gaussian and Lorentzian functions were used for peak fitting, and they gave identical results (although the Gaussian fit gave the better reduced  $\chi^2$ ).

We used deuteron spectra from the  $^{27}\text{Al}(p,d)^{26}\text{Al}$  and  $^{25}\text{Mg}(p,d)^{24}\text{Mg}$  reactions to perform two independent momentum calibrations of our focal plane, for each of the two scattering angles. The deuteron spectra at  $15^\circ$  are shown in Fig. 3. Explicitly, polynomial functions of the position  $x$  along the focal plane were fit to the momenta (or equivalently the magnetic rigidities  $B\rho$ ) of those deuteron groups corresponding to 14 states ( $2.3 < E_x < 7.3$  MeV, with  $\Delta E_x = 0.02$ – $0.07$  keV) and 12 states ( $8.8 < E_x < 13.8$  MeV, with  $\Delta E_x = 0.08$ – $3$  keV) in  $^{26}\text{Al}$  and  $^{24}\text{Mg}$ , respectively [13]. Judging by the reduced  $\chi^2$  parameter, we found that second-degree polynomials (in  $x$ ) gave the best fit to each set of  $(p,d)$  data. Figure 4 gives an indication of how good the fits are to the data at  $15^\circ$ : we plot the residuals  $\delta = (\rho_{\text{expt}} - \rho_{\text{fit}})$  divided by their  $1\sigma$  error against the position  $x$ . This  $1\sigma$  error had contributions from both the error in the excitation energy assigned to a calibration peak (from [13]) and the error due to the widths of the calibration peaks, with the latter dominating. We see that for both calibrations at  $15^\circ$ , the residuals for the various deuteron groups lie mostly within  $\pm 1\sigma$ ; this result was echoed for the two deuteron calibrations at  $25^\circ$ .

To obtain a more precise value for the scattering angle  $\theta$ , we relied on proton momentum spectra from  $(p,p')$  reactions

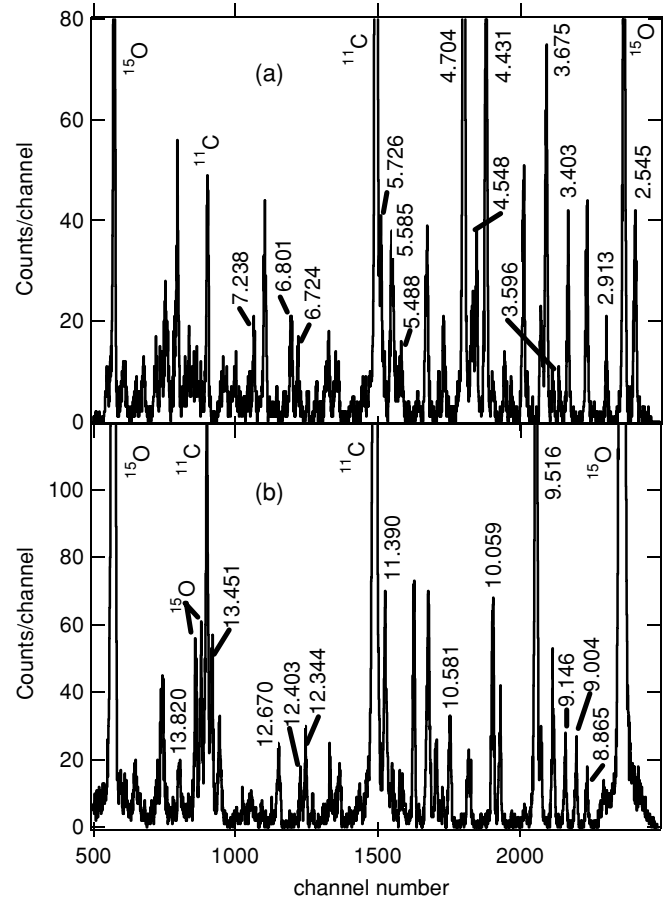


FIG. 3. Deuteron momentum spectra (at  $\theta = 15^\circ$ ) from  $(p,d)$  reactions on (a) the Al target and (b) the  $^{25}\text{MgO}$  target. These spectra were used for momentum calibration of the focal plane via the  $^{27}\text{Al}(p,d)^{26}\text{Al}$  and  $^{25}\text{Mg}(p,d)^{24}\text{Mg}$  reactions; calibration peaks are labeled by their associated  $E_x$  (in MeV, from [13]) in the respective residual nuclei. Contaminant peaks from the  $^{12}\text{C}(p,d)^{11}\text{C}$  and  $^{16}\text{O}(p,d)^{15}\text{O}$  reactions are also identified in these spectra by the appropriate residual nucleus. Peaks used for calibration were chosen based on shape, unambiguity in identification, known precision of the associated  $E_x$  in the respective residual nuclei, and the desire to utilize calibration peaks that surround the  $^{22}\text{Mg}(\text{g.s.})$ ,  $^{26}\text{Si}(\text{g.s.})$ , and  $^{14}\text{O}(\text{g.s.})$  peaks from the  $(p,t)$  spectra (see Fig. 2 and Sec. II of the text).

on the  $^{24}\text{MgO}$  target. At  $15^\circ$ , we observed protons corresponding to several states from  $^{24}\text{Mg}(p,p')^{24}\text{Mg}$ ,  $^{16}\text{O}(p,p')^{16}\text{O}$ , and  $^{12}\text{C}(p,p')^{12}\text{C}$ , along with the protons from  $^1\text{H}(p,p)^1\text{H}$  elastic scattering. We fit the magnetic rigidities of the observed states in each case with a second-degree polynomial. Since the kinematics of the observed  $(p,p')$  reactions are rather different, one can use the difference in  $B\rho$  between proton groups from the different reactions to obtain a precise value of  $\theta$  (assuming the beam energy is known). Using the 4.238 MeV state from the  $^{24}\text{Mg}(p,p')$  reaction along with the 4.439 MeV state from the  $^{12}\text{C}(p,p')$  reaction, we found  $\theta = 14.93(3)$  and  $\theta = 25.06(3)$  degrees with the data at the nominal angles of  $15^\circ$  and  $25^\circ$ , respectively (for a beam energy of 33 MeV). In principle, one should be able to improve on the precision of this value by using the  $^{12}\text{C}(p,p')$  state

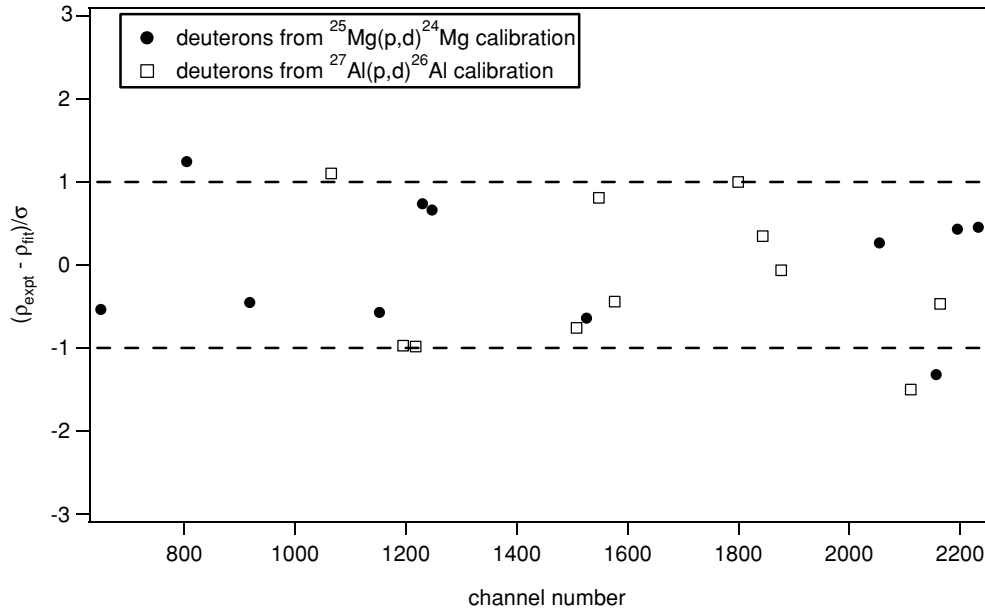


FIG. 4. The quantity  $\delta = (\rho_{\text{expt}} - \rho_{\text{fit}})$  represents the residuals from second-degree polynomial fits to the momenta of the deuterons from  $^{27}\text{Al}(p, d)^{26}\text{Al}$  (open squares) and  $^{25}\text{Mg}(p, d)^{24}\text{Mg}$  (filled circles). We divided  $\delta$  by the  $1\sigma$  error in this quantity introduced from both the fit parameters and the peak widths in the deuteron spectra; this is plotted against channel number. The scatter in  $\delta$  is contained, for the most part, within  $\pm 1\sigma$ . These fits were to the deuteron spectra at  $\theta = 15^\circ$ ; the residuals from the fits to the deuteron spectra at  $\theta = 25^\circ$  were scattered similarly.

along with the  $^1\text{H}(p, p)$  state (as the kinematics of these two reactions differ even more). However, for the data at  $25^\circ$ , the  $^1\text{H}(p, p)$  peak merged with a peak from  $^{16}\text{O}(p, p')$ ; at  $15^\circ$ , we found that the additional uncertainty in determining the centroid of the broad elastic peak from  $^1\text{H}(p, p)$  led to the same uncertainty in  $\theta$  as above (along with the same actual angle).

To better determine the beam energy, we relied on our expectation that the shape of the focal plane (namely  $d\rho/dx$  and  $d^2\rho/dx^2$  for a second-degree fit of the magnetic rigidity to position along the focal plane) be consistent among different particle groups. For a given  $\theta$ , then, one could vary the beam energy used in individual deuteron and triton momentum calibrations until their shapes were consistent. Doing this for each of the two deuteron calibrations (at  $15^\circ$ ) in conjunction with a second-degree polynomial fit to triton spectra from  $^{25}\text{Mg}(p, t)^{23}\text{Mg}$ , we found that  $|\frac{d\rho}{(dx)_{\text{deuteron}}} - \frac{d\rho}{(dx)_{\text{triton}}}|$  was minimized with respect to the beam energy at  $E_{\text{beam}} = 32.994(5)$  MeV for  $^{25}\text{Mg}(p, d)$  and  $E_{\text{beam}} = 32.996(5)$  MeV for  $^{27}\text{Al}(p, d)$ . (The values of  $d^2\rho/dx^2$  for the three fits were constant and consistent as we varied the beam energy from 32.980 to 33.020 MeV, so we only needed to check the  $d\rho/dx$  factors for agreement in the shape of the focal plane between deuterons and tritons.) Repeating this for the deuteron calibrations at  $25^\circ$ , we found beam energies of  $E_{\text{beam}} = 32.996(5)$  MeV for  $^{25}\text{Mg}(p, d)$  and  $E_{\text{beam}} = 32.993(5)$  MeV for  $^{27}\text{Al}(p, d)$ . The scattering angle results described above were unchanged when these new beam energies were used in that calculation.

We note that the constant terms in the fits to the deuteron and triton momenta differed. We attribute this effect to imperfections in the constant fraction discriminators (CFDs)

used with our focal plane detector. Since our gas-filled detector works in delay-line mode, we detect the position of a particle through an electron avalanche as it drifts past a wire (the idealized focal plane) held at high voltage. Protons, deuterons, and tritons entering our detector all lose different amounts of energy in the gas. This may lead an imperfect CFD to trigger on  $\alpha$  particles some nanoseconds before it triggers on protons; effectively, the focal planes for the different particle types are staggered. The end result is that particles of different mass, but the same momentum (or  $\rho$ ) will register different positions  $x$ . This is a small effect (amounting to a difference of one to two channels for deuterons and tritons of the same  $\rho$ ); however, the precision desired for these mass measurements forces us to carefully examine this problem.

Because of this issue, the deuteron calibrations cannot be used to directly determine the absolute magnetic rigidities of the tritons from the  $^{24}\text{Mg}(p, t)$  and  $^{28}\text{Si}(p, t)$  data. We can, however, make a relative measurement since the *shape* of the focal plane is consistent among deuterons and tritons even if the overall constants in the fits differ. Following this idea, we used each deuteron calibration (at each of the two scattering angles) to determine the magnetic rigidities of the triton peaks corresponding to the ground states of  $^{22}\text{Mg}$ ,  $^{26}\text{Si}$ , and  $^{14}\text{O}$ . (Recall that the  $^{14}\text{O}$  ground state appeared in the spectra from both the  $^{24}\text{Mg}(p, t)$  and  $^{28}\text{Si}(p, t)$  reactions—see Fig. 2.) Using the beam energy and scattering angle, we then calculated the  $Q_0$  values of  $^{24}\text{Mg}(p, t)^{22}\text{Mg}$  and  $^{28}\text{Si}(p, t)^{26}\text{Si}$  relative to that of  $^{16}\text{O}(p, t)^{14}\text{O}$ . Finally, we assumed the mass table values [14] of  $^{24}\text{Mg}$ ,  $^{28}\text{Si}$ ,  $^{16}\text{O}$ ,  $^{14}\text{O}$ ,  $p$ , and  $t$  to obtain the mass excesses of  $^{22}\text{Mg}$  and  $^{26}\text{Si}$ . These are given in Table III, along with their respective statistical and systematic uncertainties.

TABLE III. Mass excesses  $\Delta$  of  $^{22}\text{Mg}$  and  $^{26}\text{Si}$  from the two independent deuteron calibrations of the focal plane, at each of the two scattering angles. The uncertainties  $\sigma_{\text{stat}}$  and  $\sigma_{\text{sys}}$  represent statistical error [due to the number of counts in the  $^{24}\text{Mg}(p,t)^{22}\text{Mg}(\text{g.s.})$  or  $^{28}\text{Si}(p,t)^{26}\text{Si}(\text{g.s.})$  and  $^{16}\text{O}(p,t)^{14}\text{O}(\text{g.s.})$  peaks—see Fig. 2] and systematic error (from varying the beam energy by  $\pm 5$  keV, the scattering angle by  $\pm 0.03^\circ$ , and the target thicknesses by  $\pm 15\%$ ).

Calibration	Angle	$^{22}\text{Mg}$			$^{26}\text{Si}$		
		$\Delta(\text{keV})$	$\sigma_{\text{stat}}(\text{keV})$	$\sigma_{\text{sys}}(\text{keV})$	$\Delta(\text{keV})$	$\sigma_{\text{stat}}(\text{keV})$	$\sigma_{\text{sys}}(\text{keV})$
$^{25}\text{Mg}(p,d)^{24}\text{Mg}$	$15^\circ$	-399.4	0.4	0.3	-7138.5	0.6	0.3
	$25^\circ$	-401.6	0.3	0.4	-7140.6	0.7	0.5
$^{27}\text{Al}(p,d)^{26}\text{Al}$	$15^\circ$	-400.9	0.4	0.3	-7140.2	0.6	0.3
	$25^\circ$	-399.9	0.3	0.4	-7138.6	0.7	0.5

Given the differences in the results from the calibrations, we extract from our  $(p,t)$  data mass excesses for  $^{22}\text{Mg}$  and  $^{26}\text{Si}$  of  $-400.5(1.0)$  and  $-7139.5(1.0)$  keV, respectively. For comparison, the mass excesses from the 2003 mass evaluation [14] are  $-397.0(1.3)$  keV for  $^{22}\text{Mg}$  (see Fig. 1 for other more recent measurements) and  $-7145(3)$  keV for  $^{26}\text{Si}$ .

### III. DISCUSSION

As shown in Fig. 1, our result for the mass of  $^{22}\text{Mg}$  is in excellent agreement with the re-evaluation of an older determination of the  $^{22}\text{Mg}$  mass [16] and the recent high-precision Penning trap mass measurements [17,18]. We note that the TRIUMF measurement of  $E_R$  for the  $E_x = 5.71$  MeV state in  $^{22}\text{Mg}$  [12] requires a measurement of the excitation energy of that state to yield a determination of the  $^{22}\text{Mg}$  mass. If one uses the two recent  $\gamma$ -ray measurements from the  $E_x = 5.71$  MeV state of  $^{22}\text{Mg}$  (see Table II), in conjunction with the  $E_R$  measurement, one obtains agreement among all the recent efforts to determine the  $^{22}\text{Mg}$  mass.

With regard to the mass of  $^{26}\text{Si}$ , the only measurement used in the 2003 mass evaluation [14] is from [15], where the  $Q_0$  value of the  $^{28}\text{Si}(p,t)^{26}\text{Si}$  reaction was measured as  $-22009(3)$  keV. Using this with current masses of  $^{28}\text{Si}$ ,  $p$  and  $t$  [14], we find the mass excess of  $^{26}\text{Si}$  as  $-7145(3)$  (which is the value in the 2003 mass evaluation). A recent re-calibration of this measurement yields  $-7145.5(3.0)$  keV [24]. Support for our determination of the  $^{26}\text{Si}$  mass excess

TABLE IV. Low-energy resonance parameters for  $^{25}\text{Al}(p,\gamma)^{26}\text{Si}$ , using our  $^{26}\text{Si}$  mass excess of  $-7139.5$  keV. Values for  $E_x$  are from a weighted average of the results in [7–9]; we chose the  $J^\pi$  assignments to these states following [7] and [8].  $E_R^{\text{new}}$  was found from  $E_x$  assuming our  $^{26}\text{Si}$  mass measurement. The proton partial widths  $\Gamma_p^{\text{new}}$  are based on those from [25], but have been modified following [26] to take into account the changed resonance energy;  $\Gamma_\gamma$  is directly from [25].

$E_x(\text{keV})$	$J^\pi$	$E_R^{\text{new}}(\text{keV})$	$\Gamma_p^{\text{new}}(\text{eV})$	$\Gamma_\gamma(\text{eV})$	$\omega\gamma^{\text{new}}(\text{eV})$
5517(3)	$4^+$	4	$\sim 10^{-80}$	0.0066	$\sim 10^{-80}$
5672(4)	$1^+$	159	$4.5 \times 10^{-9}$	0.11	$1.1 \times 10^{-9}$
5915(2)	$0^+$	403	0.011	0.0088	$4.1 \times 10^{-4}$
5946(4)	$3^+$	434	6.3	0.033	$1.9 \times 10^{-2}$

as  $-7139.5(1.0)$  keV is provided by the good agreement of our  $^{22}\text{Mg}$  mass measurement with the two recent Penning trap results for  $^{22}\text{Mg}$ . More studies of the mass of  $^{26}\text{Si}$  are clearly needed to help clarify the 6 keV discrepancy we find between our measurement and that of [24].

To explore the implications of our result on nucleosynthesis in novae, we calculate the resonant reaction rate of

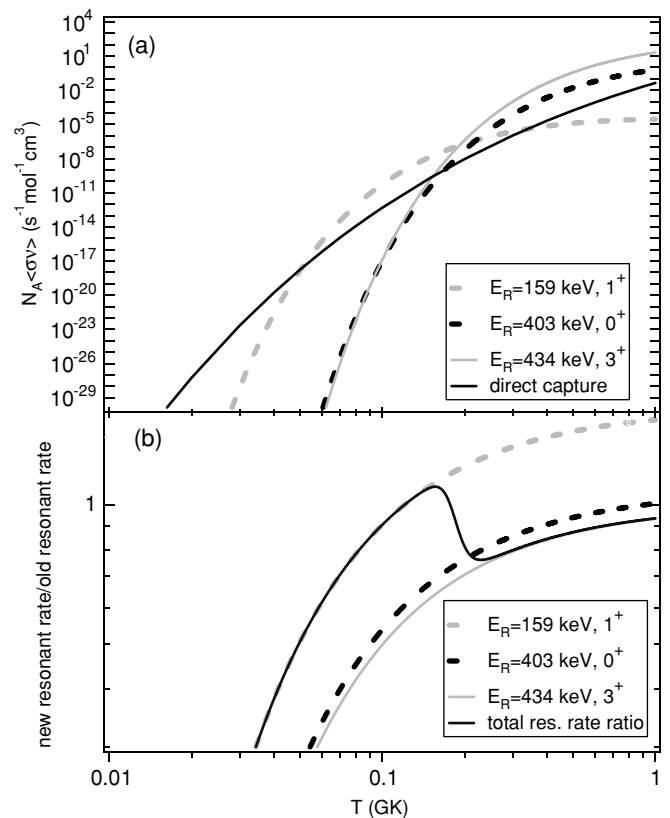


FIG. 5. (a) Contributions to the total reaction rate of  $^{25}\text{Al}(p,\gamma)^{26}\text{Si}$  at nova temperatures, assuming our  $^{26}\text{Si}$  mass excess of  $-7139.5$  keV. We show the unnatural parity states as the major contributors to the resonant reaction rate at nova temperatures ( $0.1 < T < 0.4$  GK), in agreement with [7] and [9]. Parameters used in the calculations can be found in Table IV. The direct capture component is given in [25]. (b) Ratio of the resonant contributions to the total rate assuming our new  $^{26}\text{Si}$  mass, to the equivalent quantities assuming the 2003 mass evaluation for the  $^{26}\text{Si}$  mass excess ( $-7145$  keV [14]).

$^{25}\text{Al}(p,\gamma)^{26}\text{Si}$  using our  $^{26}\text{Si}$  mass compared to that using the 2003 mass evaluation. For nova temperatures ( $0.1 < T < 0.4$  GK) it is sufficient to consider only those resonances in  $^{26}\text{Si}$  with  $E_R < 600$  keV [8]; Table IV lists these resonances and their properties that we used in the rate calculation. Relevant formulas are given in [25]. For the excitation energies  $E_x$  of the four resonances in the region of interest, we have used weighted averages of the measurements from [7–9]; we have chosen the spin-parity assignments of [7,8] for these states. We converted  $E_x$  to  $E_R$  by using both  $Q_0^{\text{old}} = 5517.7$  keV (the  $^{25}\text{Al}(p,\gamma)^{26}\text{Si}$   $Q_0$  value using [14] for all masses) and  $Q_0^{\text{new}} = 5512.3$  keV (the  $Q_0$  value using our measurement of the  $^{26}\text{Si}$  mass along with [14] for the masses of  $^{25}\text{Al}$  and  $p$ ). The  $\gamma$  partial widths  $\Gamma_\gamma$  used are based on shell model calculations and experimental values from  $^{26}\text{Mg}$ ; they have been taken directly from [25]. Proton partial widths  $\Gamma_p$  in Table IV are based on those calculated in [25], but have been modified in proportion to the Gamow factor (see [26]) to account for the changes in  $E_R$ .

Figure 5(a) shows the contributions to the resonant rate of  $^{25}\text{Al}(p,\gamma)^{26}\text{Si}$  by the  $0^+$ ,  $1^+$ , and  $3^+$  states in  $^{26}\text{Si}$ —the  $4^+$  state is too close to the  $^{25}\text{Al} + p$  threshold to be a factor. These calculations are based on our new measurement of the  $^{26}\text{Si}$

mass and use the parameters in Table IV. The direct capture (DC) component is also shown; this has been calculated in [25]. We see that the unnatural parity contributions to the total rate dominate at nova temperatures, in agreement with the results of [7] and [9]. Figure 5(b) gives the ratio of the results in Fig. 5(a) to resonant rate calculations using the 2003 mass evaluation [14] for the  $^{26}\text{Si}$  mass. For  $T < 0.04$  GK, the resonant rate is reduced significantly by the new  $^{26}\text{Si}$  mass; however, we see from Fig. 5(a) that the DC component dominates in this regime. For  $T > 0.2$  GK, we see that the total resonant rate (and hence the total rate since the DC contribution is minor for  $T > 0.04$  GK) is reduced by as much as 30% using our  $^{26}\text{Si}$  mass. Additional measurements of  $^{26}\text{Si}$  states above the  $^{25}\text{Al} + p$  threshold, as well as experimental results for the  $\gamma$  and proton partial decay widths of these states would help put these indirect rate calculations on firmer ground.

#### ACKNOWLEDGMENTS

We gratefully acknowledge Ted Rounsaville for his work building the focal plane detector. This work was supported by the U.S. Department of Energy, Grant No. DE-FG02-91ER-40609 and Contract No. W-31-109-ENG-38.

- 
- [1] M. Hernanz and J. Jose, *New Astron. Rev.* **48**, 35 (2004).
  - [2] R. Diehl *et al.*, *Astron. Astrophys.* **298**, 445 (1995).
  - [3] R. Diehl *et al.*, *Astron. Astrophys.* **411**, L451 (2003), and references therein.
  - [4] A. F. Iyudin *et al.*, *Astron. Astrophys.* **300**, 422 (1995).
  - [5] R. Diehl, N. Prantzos, and P. von Ballmoos, *Nucl. Phys. A* (to be published).
  - [6] J. M. D’Auria *et al.*, *Phys. Rev. C* **69**, 065803 (2004), and references therein.
  - [7] J. A. Caggiano, W. Bradfield-Smith, R. Lewis, P. D. Parker, D. W. Visser, J. P. Greene, K. E. Rehm, D. W. Bardayan, and A. E. Champagne, *Phys. Rev. C* **65**, 055801 (2002).
  - [8] D. W. Bardayan *et al.*, *Phys. Rev. C* **65**, 032801(R) (2002).
  - [9] Y. Parpottas, S. M. Grimes, S. Al-Quraishi, C. R. Brune, T. N. Massey, J. E. Oldendick, A. Salas, and R. T. Wheeler, *Phys. Rev. C* **70**, 065805 (2004).
  - [10] J. Jose, A. Coc, and M. Hernanz, *Astrophys. J.* **520**, 347 (1999).
  - [11] C. Iliadis, A. E. Champagne, J. Jose, S. Starrfield, and P. Tupper, *Astrophys. J. Suppl.* **142**, 105 (2002).
  - [12] S. Bishop *et al.*, *Phys. Rev. Lett.* **90**, 162501 (2003).
  - [13] P. M. Endt, *Nucl. Phys.* **A521**, 1 (1990), and references therein.
  - [14] G. Audi, A. H. Wapstra, and C. Thibault, *Nucl. Phys.* **A729**, 337 (2003).
  - [15] J. C. Hardy, G. Schmeing, W. Benenson, G. M. Crawley, E. Kashy, and H. Nann, *Phys. Rev. C* **9**, 252 (1974).
  - [16] J. C. Hardy *et al.*, *Phys. Rev. Lett.* **91**, 082501 (2003).
  - [17] G. Savard *et al.*, *Phys. Rev. C* **70**, 042501(R) (2004).
  - [18] M. Mukherjee *et al.*, *Phys. Rev. Lett.* **93**, 150801 (2004).
  - [19] D. Seweryniak *et al.*, *Phys. Rev. Lett.* **94**, 032501 (2005).
  - [20] C. Jewett (private communication).
  - [21] A. A. Chen *et al.*, TRIUMF EEC proposal E922 (unpublished).
  - [22] A. Parikh *et al.*, *Nucl. Instrum. Methods* (in preparation).
  - [23] A. A. Chen, Ph.D. thesis, Yale University, 1999.
  - [24] J. C. Hardy (private communication).
  - [25] C. Iliadis, L. Buchmann, P. M. Endt, H. Herndl, and M. Wiescher, *Phys. Rev. C* **53**, 475 (1996).
  - [26] C. E. Rolfs and W. S. Rodney, *Cauldrons in the Cosmos* (University of Chicago Press, Chicago, 1988).